Relationships between precipitating auroral zone electrons and lower thermospheric nitric oxide densities: 1998 – 2000

D.N. Baker,[1] C.A. Barth,[1] K.E. Mankoff,[1] S.G. Kanekal,[1] S.M. Bailey,[2] G.M. Mason,[3] and J.E. Mazur[4]

Abstract. Data acquired using the Student Nitric Oxide Explorer (SNOE) spacecraft during the years 1998-2000 are presented for nitric oxide (NO) measured at altitudes between 90 and 170 km. These data are compared with energetic electron fluxes ($E>25$ keV) measured concurrently using a large-area microchannel plate sensor system (Low-Energy Ion Composition Analyzer) (LICA) on board the Solar, Anomalous, and Magnetospheric Particle Explorer (SAMPEX) spacecraft. Three geomagnetic storm intervals (in May 1998, September 1998, and October 1998) are examined specifically to determine altitude and latitude variations of NO production as it compares to energetic electron precipitation. A broader statistical analysis is then carried out using daily averages of peak NO densities (at 106 km altitudes) and electron intensities measured by SAMPEX. Northern and Southern Hemisphere data are treated separately within the magnetic latitude bands 60°-70° north and south. We find correlation coefficients of 0.56 (north) and 0.73 (south) for NO density versus SAMPEX electron count rates using two complete years of data. We also use the National Oceanic and Atmospheric Administration (NOAA) "hemispherical power index" to compare with SAMPEX and with SNOE measurements. Correlation coefficients of ~0.6 are found among all the daily-averaged quantities, suggesting that perhaps 30-40% of the variance in NO density can be accounted for by the particle measurements used. An analysis and adjustment of NO densities to account for seasonal effects increases the NO correlations with particle intensities to ≥ 0.7.

1. Introduction

There has been increasing attention paid in recent years to the "last leg" of the Sun-Earth connection, namely, the precipitation of energetic magnetospheric particles into the Earth's upper and middle atmosphere. Early suggestions [e.g., *Thorne*, 1977; *Baker et al.*, 1987] were made that relativistic electrons ($E \gtrsim 0.5$ MeV) could couple radiation belt variations directly into the middle atmosphere both by changing the lower ionospheric electrical conductivity and by altering the atmospheric molecular chemistry. This chemical aspect of magnetosphere-atmosphere coupling has been pursued quite extensively using both observational data and large-scale numerical models [*Callis et al.*, 1991, 1996, 1998]. There is good evidence from this work that energetic electron precipitation has a clear and significant effect in terms of mesospheric odd-nitrogen (NO_y) production. Moreover, downward transport of this NO_y, especially in the winter polar regions, has been shown to have a clear subsequent influence on stratospheric ozone levels [*Callis et al.*, 1998; *Randall et al.*, 1998; also C.E. Randall et al., Validation of POAM III NO_2, submitted to *Journal*

of *Geophysical Research*, 2001]. Thus the picture of catalytic destruction of ozone by oxides of nitrogen seems to be an important aspect of atmospheric change to consider along with direct solar influences and anthropogenic changes [e.g., *Lean et al.*, 1994].

Whereas early work on middle atmospheric chemical changes induced by particle precipitation focused on relativistic electrons [*Thorne*, 1977] or solar energetic particles [e.g., *Crutzen et al.*, 1975], more recent work has emphasized the importance of considering the entire precipitating electron spectrum from $E \sim 1.0$ keV to $E \sim 1$ MeV [*Callis et al.*, 1998]. The lower-energy end of the precipitating electron spectrum has long been recognized as producing copious quantities of nitric oxide (NO) and other nitrogen compounds in the lower thermosphere [e.g., *Barth*, 1992; *Roble*, 1992]. One of the challenges of understanding the effects of precipitating electrons on atmospheric chemistry has been to acquire a continuous record of thermospheric NO densities concurrent with a measure of precipitating electrons.

Although NO is a minor constituent in the lower thermosphere (having concentrations of ~10-100 ppm), it nonetheless plays a key role in the atmosphere because of its chemical and physical properties [e.g., *Codrescu et al.*, 1997; *Ridley et al.*, 1999; *Crowley et al.*, 1999]. Because of its relatively low ionization potential, the ions produced by photoionization of major thermospheric constituents readily transfer their charge to NO. This makes NO ions the major ion species in the lower ionosphere. Furthermore, since NO molecules radiate strongly in the IR portion of the electromagnetic spectrum, they play a significant role in determining the thermal structure of the thermosphere. As noted above, the nitric oxide produced in the lower thermosphere is a form of odd nitrogen which can be transported downward into the mesosphere and stratosphere [*Barth et al.*, 1999; *Callis et*

[1] Laboratory for Atmospheric and Space Physics, University of Colorado, Boulder, Colorado, USA.
[2] Center for Atmospheric Sciences, Hampton University, Hampton, Virginia, USA.
[3] Department of Physics, University of Maryland, College Park, Maryland, USA.
[4] Aerospace Corporation, El Segundo, California, USA.

al., 1998]. There it can play a major part in the catalytic destruction of ozone (O_3).

This paper utilizes continuous data from the Student Nitric Oxide Explorer (SNOE) spacecraft along with electron data from the Solar, Anomalous, and Magnetospheric Particle Explorer (SAMPEX) to carry out case study and statistical analyses of relationships between particle precipitation and NO production.

2. Data Sets and Instrumentation

Nitric oxide for this study was measured in a broad range of latitudes using the Student Nitric Oxide Explorer satellite [*Barth et al.*, 1999]. The NO density is determined with an ultraviolet spectrometer (UVS) from the fluorescence scattering of ultraviolet sunlight by nitric oxide, The SNOE satellite is in a nearly circular, Sun-synchronous orbit at an altitude of 556 km with an orbital period of 96 min and an inclination of 97.75°. Using the spinning motion of the satellite, the UVS telescope scans the limb five times per minute, producing altitude profiles of the NO density between 90 and 170 km. The nitric oxide is measured on the daylight portion of the orbit at 1030 LT. SNOE has returned data continuously since its launch in February 1998.

The SAMPEX spacecraft was launched in July 1992 into a low-Earth orbit with an inclination of 81.7° and an altitude range of 520 x 675 km [see *Baker et al.*, 1993]. There are four science instruments on board SAMPEX measuring a wide variety of energetic ions as well as the broad spectrum of energetic electrons. The Low-Energy Ion Composition Analyzer (LICA) is designed principally as a time-of-flight and residual energy detector telescope to measure energetic ion composition. However, the time-of-flight start (and stop) chevron microchannel plate (MCP) sensors provide a large-area, sensitive particle detection system. The start MCP sensor detects electrons with $E>25$ keV and has a geometric factor $g\sim50$ cm^2 sr. (The sensor is also sensitive to protons with $E>250$ keV, but throughout most of the SAMPEX orbit the response is dominantly due to suprathermal electrons.) A full description of the LICA sensor system is given by *Mason et al.* [1993]. Because of its relatively broad angular response, LICA measures both trapped and precipitating electrons at most SAMPEX orbital locations. However, our tracing analysis shows that at midlatitudes to high latitudes the particle count rates presented here are due to particles either in the bounce loss cone, or else in the drift loss cone. Thus the LICA rates are indicative of particles that rather rapidly enter the atmosphere. In this paper, we interpret the LICA MCP singles counting rate data (corrected for known backgrounds, etc.) as a sensitive measure of precipitating electrons with $E>25$ keV.

Given that SNOE and SAMPEX both operate at very similar altitudes, and both are in highly inclined orbits, it is of interest to intercompare their data. Note, however, that SAMPEX is not Sun-synchronous and, therefore, its orbit precesses in local time: The SAMPEX orbital plane moves through all local times in about 3 months. On the other hand, SNOE is Sun-synchronous and always moves in the 1030-2230 LT plane. Both SNOE and SAMPEX complete roughly 15 orbits per day and thereby sample geographic longitude bands that are separated by about 24° from one orbit to the next. In this paper we bin data from the two spacecraft into 5° latitude bins and we use primarily daily averages of NO density and electron flux, which means that we average over all longitudes.

3. Overview of Data Sets

Plate 1 is a color-coded representation of data for 1998, 1999, and 2000 for SAMPEX LICA (top panel) and for SNOE UVS (bottom panel). The data are plotted in each case with geomagnetic latitude as the vertical scale and time (in days of year) as the horizontal scale. The scale of the color coding for the respective panels is given by the color bars to the right of the image. Each vertical stripe in the panels of Plate 1 summarizes the average electron counting rate or NO density (at 106 km) for each day.

Notice that the LICA measurements extend from pole to pole, while the SNOE data show gaps near the poles (which broaden during times of winter in the respective hemispheres). This feature of SNOE data simply reflects the fact that the NO measurements are made in daylight periods using limb scanning of solar fluorescence. SAMPEX, on the other hand, is able to measure precipitating electrons all the way to the geomagnetic poles (on at least some orbits) every day.

In general, Plate 1 shows a correspondence between intense electron events detected by SAMPEX LICA and NO density enhancements detected by SNOE. However, there are some intervals where NO densities were low and electron intensities were high and vice versa. Nonetheless, the overwhelming impression from comparing the SNOE and SAMPEX measurements is that both sensor systems are dominantly responding within the band of geomagnetic latitudes associated with the auroral zones, that is, magnetic latitude (MLAT) ~60°-70° [see *Barth et al.*, 2001]. It is natural to presume that the SNOE measurements are related to electron-induced production of NO by ~1-10 keV electrons [*Barth*, 1992; *Barth et al.*, 2001], while the LICA-measured electrons $E>25$ keV are the high-energy "tail" of the auroral electron population.

There are several intense NO events and electron precipitation events evident in Plate 1 which correspond to well-studied geomagnetic storm intervals. In the following section, we investigate three 1998 storm-related periods in greater detail.

4. Geomagnetic Storm Intervals in 1998

As is evident from the data in Plate 1, there were several intense events in the spring and fall seasons of 1998. These events were associated with relatively strong geomagnetic storm intervals that have been the focus of major organized community analysis efforts. The storm in May 1998 is at the core of the Solar-Terrestrial Energy Program (STEP)-Results, Applications, and Modeling Phase (S-RAMP) special analysis interval. The S-RAMP program is carried out under the aegis of the Scientific Committee on Solar-Terrestrial Physics (SCOSTEP) and it has selected April-May 1998 as an analysis interval for special space weather investigation [see *Baker et al.*, 1998; *Baker*, 2000]. Geomagnetic storms in September and October 1998 have been selected for study in the Geospace Environment Modeling (GEM) program "Inner Magnetosphere" Campaign [see *McAdams and Reeves*, 2001, and references therein].

In this section, analyses are presented for each of the selected geomagnetic storm intervals. Information is presented about solar wind and geomagnetic conditions, and then comparisons are made between SNOE and SAMPEX measurements during the course of each storm period.

4.1. Case Study: May 1-7, 1998

The active Sun in April-May 1998 produced powerful streams of solar wind plasma that were detected upstream of the Earth. Figure 1 shows the solar wind speed (V), the interplanetary plasma density (N), and the interplanetary magnetic field (IMF) north-south component (B_z) for the period May 1-5, 1998 (similar to Figure 9 of *Baker* [2000]). Several separate streams were seen
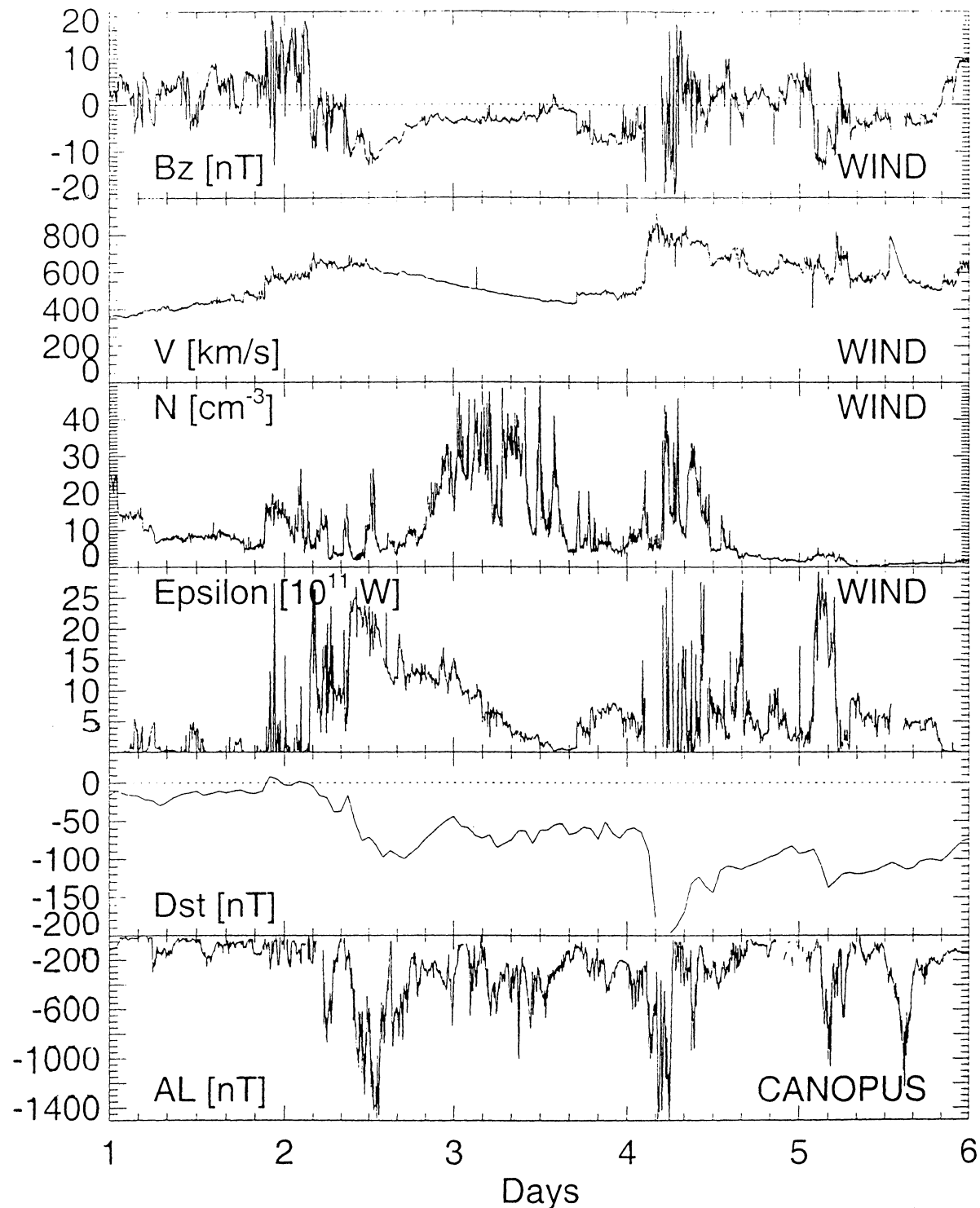
Figure 1. Interplanetary magnetic field B_z component and solar wind speed and density (top three panels, respectively) for the period May 1-5 1998 (Data courtesy of R.P. Lepping and K. Ogilvie, 1999). The fourth panel shows the "energy coupling" parameter ε for the same period, while the lower two panels show the Dst and auroral electrojet indices (the latter derived from the Canadian Auroral Network for the OPEN Program Unified Study (CANOPUS) chain of magnetometers). A powerful series of solar wind and geomagnetic disturbances were seen including a major geomagnetic storm development on May 4 (day 124).

in which V reached peak values ≥ 600 km/s. Such streams are very effective at producing subsequent magnetospheric high-energy electron events. A notable solar wind period occurred on May 4 when V went to ~850 km/s. This was the highest solar wind speed that had been measured near 1 AU in the prior several years [*Baker et al.*, 1998; *Baker*, 2000] and was probably caused by a coronal mass ejection (CME) event seen in Solar and Heliospheric Observatory (SOHO) coronagraph data [*Baker*, 2000].

Powerful geomagnetic activity and electron acceleration are expected when high solar wind speed occurs in combination with

large B_{IMF}, and especially when the interplanetary B_z is strongly negative. The planetary magnetic index Kp reached a level of 9 on May 4. The second panel from the bottom in Figure 1 shows that the Dst index on that day reached values less than -200 nT (a major geomagnetic storm) and the provisional auroral electrojet (AL) index reached <-1400 (see bottom panel of Figure 1).

Ground-based observations (see Dst in Figure 1) and in situ ion data from the POLAR spacecraft show a very strong ring current response to the solar wind conditions in early May 1998 [*Baker*, 2000]. On May 2, the ring current underwent its first intensification, corresponding to a Dst of around -100 nT. The second, larger intensification, followed shortly after the e ($=VB^2 \ell o^2 \sin^4 (\theta/2)$, where q is the angle between the z direction and the IMF projection in the y-z (GSM) plane) parameter reached nearly 10^4 GW, and resulted in a (pressure-corrected) Dst value of -250 nT. The ring current energy at the peak of the storm was about 4 x 10^{15} J. Generally, the data show a good agreement between Dst and the measured ring current energy from POLAR [*Baker et al.*, 2001].

The May 1998 storm produced very large inputs of energy into the auroral ionosphere due to Joule heating and particle precipitation [*Baker et al.*, 2001]. It also caused significant changes in the chemical makeup of the lower thermosphere. Plate 2 shows a sequence of frames which illustrate the density of NO measured by SNOE during the storm. The log of nitric oxide density is shown as a daily average with the vertical axis indicating altitude and the horizontal axis indicating geomagnetic latitude. (Careful analysis shows that SNOE data exhibit a maximum correlation with SAMPEX data when lagged in time by eight orbits, or about 0.5 days. This is reasonable given the NO molecular lifetime of ~1 day in this region. Thus in all of our work we use daily averages with this eight-orbit lag built in.) Plates 2a-2d represent results for days 122 through 125 (May 2-5) of 1998, respectively. Near the top of each panel is a bar which shows the color-coded log of electron flux (E>25 keV) measured for that day by the SAMPEX LICA sensor. These electron data indicate where in geomagnetic latitude there was intense auroral electron precipitation.

As is evident from Plate 2a, there was relatively weak NO production on day 122 (May 2, i.e., prior to the geomagnetic storm development). Similarly the electron precipitation was weak on day 122. By day 123, and even more clearly by days 124 and 125 (when the geomagnetic storm activity peaked), there was a large increase in the NO production. This was plausibly caused by the increased precipitation of energetic electrons into the lower thermosphere. Note the strong north-south latitudinal asymmetries in the NO production (also seen in the precipitating electrons): Much more NO (and electron flux) was observed in the Southern Hemisphere in this case. Notice also how low in altitude and how far equatorward in latitude the NO spread during this major storm.

4.2. Case Study: September 24-28, 1998

A storm which was similar in the size of peak Dst development to that of May 4, 1998, began with a sudden storm commencement (SSC) very late on September 24, 1998. As seen from the data in Figure 2, Dst reached a maximum negative value (between -200 and -230 nT) early on day 268 (September 25) and then recovered over the next several days. The 65-station auroral electrojet (AE) index (see *Lu et al.* [1998] for description) reached values (second panel of Figure 2) above 2000 nT and the 3-hourly Kp reached values >8 on day 268. The Wind satellite data in the lower panel of Figure 2 show that the geomagnetic

storm was driven by a powerful combination of high solar wind speed (peak V_{SW} ≳850 km/s) and interplanetary magnetic field B_z values approaching -20 nT.

Plate 3 is in a format similar to that of Plate 2. Plates 3a –3d correspond to days 267-270, respectively. As seen in these SNOE altitude versus latitude plots, NO densities were relatively low on day 267 (September 24) before the geomagnetic storm developed. There were very high densities (~7 x 10^8 cm^{-3}) of NO between altitudes of ~100 km and ~120 km on days 268 and 269. These high NO densities extended equatorward (as in the May 1998 case) to geomagnetic latitudes of ~40° (north and south). The NO recovered to much lower, more typical densities by day 270. The NO profiles in Plate 3 are much more north-south symmetric than were the measured values in the May 1998 case.

The times of high NO density in this September storm interval correspond closely to the times of largest Dst development (see Figure 2). Day 268 was also the day with large AE values. We note that auroral activity, as measured by AE (as well as AU and AL), had subsided quite considerably by day 269. However, the NO persisted strongly through day 269. This is consistent with the ~0.8 day lifetime of NO at these altitudes [*Barth et al.*, 1999, 2001].

Note in Plate 3 the good correspondence between the E>25 keV electron counting rates and the NO densities. In this event interval, the electron count rates were much more symmetric (north-south) than they were in the May case. Also the electron intensities in the relatively high-energy range of LICA were more intense (and broader in latitude extent) on day 269 than on day 268. By day 270, both the NO densities and the electron intensities had substantially subsided.

4.3. Case Study: October 17-24, 1998

The third case study chosen for analysis here is another of the GEM Inner Magnetospheric Campaign intervals. As seen from the data in Figure 3, this was a much weaker storm (peak Dst ~-130 nT), but the storm recovery was rather extended in time. The major Dst development period on day 292 (October 19) was caused by a "square wave" pulse of southward IMF (B_z~-16 nT). During this day, however, V_{SW} was barely above 400 km/s. As seen in the lower panel of Figure 3, the long Dst recovery interval and the episodic enhancements of the auroral electrojets on days 293-297 were caused primarily by large (and intermittently enhanced) values of V_{SW}: At its peak (on day 295), V_{SW} reach a value of ~700 km/s.

Plate 4 is analogous in format to Plates 2 and 3. Plates 4a-4d show SNOE and SAMPEX data for days 291-294 (October 18-21). In this case, the SNOE measurements of NO density show a strong asymmetry, favoring the Northern Hemisphere over the south. This is the opposite of what was seen, for example, in the May 1998 example (Plate 2). In Plate 4, we do not see any particularly strong enhancement in the LICA counting rates (at least not comparable to the stronger May and September 1998 storms). Thus in this weaker October storm the NO density correlation with the E>25 keV electrons seems weaker. This may suggest that the auroral precipitating electron energy spectrum was much softer in this case. The highest electron counting rates for LICA were actually observed on day 293, that is, during the recovery phase of the Dst profile.

5. Statistical Analyses

As is evident from Plate 1 and from the case studies presented above, nitric oxide densities are enhanced broadly in altitude and
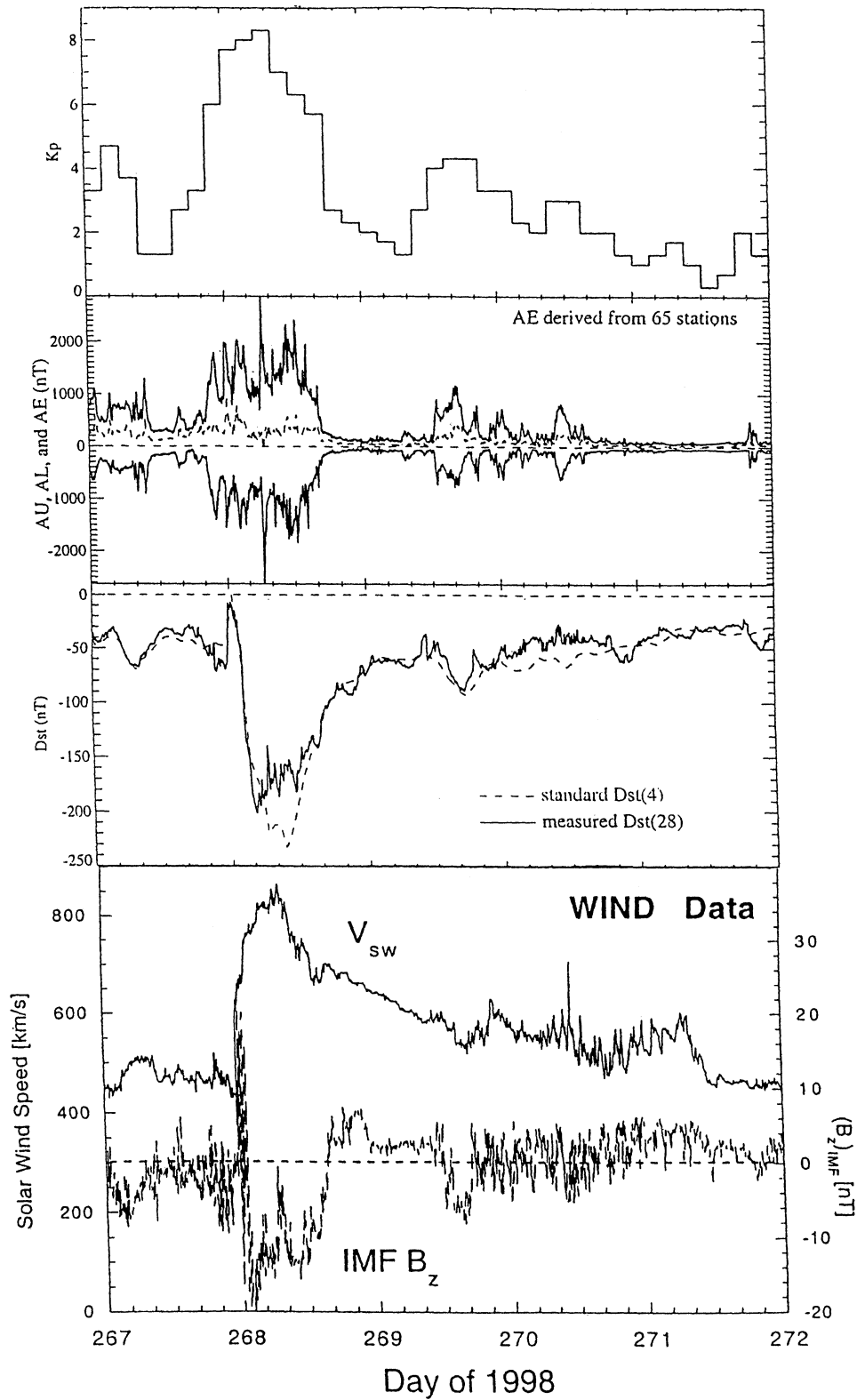
Figure 2. Interplanetary and geomagnetic data (as labeled) for the period September 24-28, 1998 (days 267-271). A major geomagnetic storm was observed on September 25 (day 268) as shown by the *Kp* and *Dst* indices.

in geomagnetic latitude during magnetic storms. Similarly, we see evidence from the LICA data that energetic electrons are enhanced in intensity during storm intervals, again over a fairly broad range of geomagnetic latitudes. However, for both NO densities and $E>25$ keV electrons, a band of latitudes ~60°-70° is representative of where peak enhancement occurs both in the Northern and Southern Hemispheres. In this section we analyze data in these latitude bands. As was also evident from Plates 2, 3, and 4 (as well as earlier work [*Barth et al.*, 1999]), the typical peak in NO density occurs around an altitude of 106 km. We use
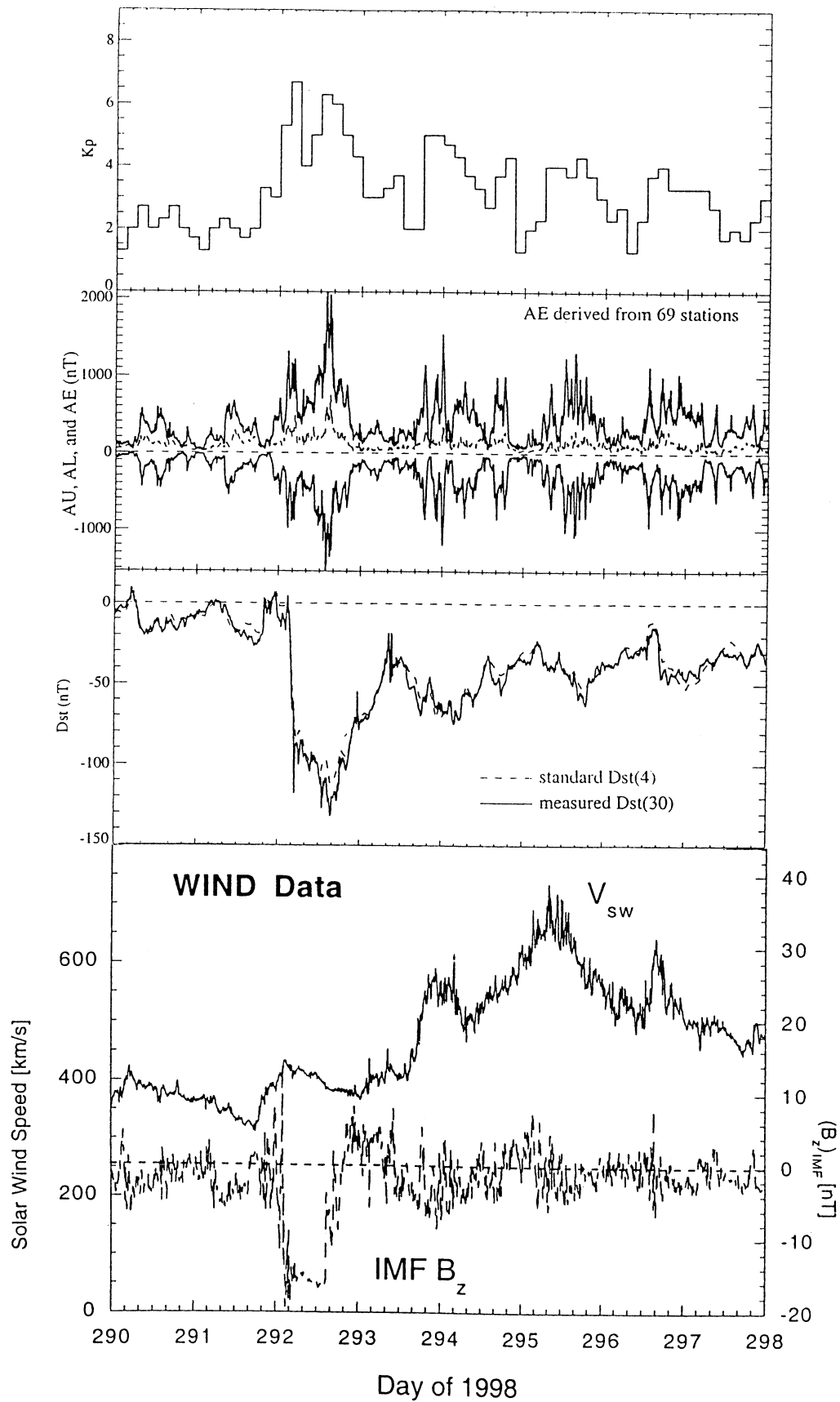
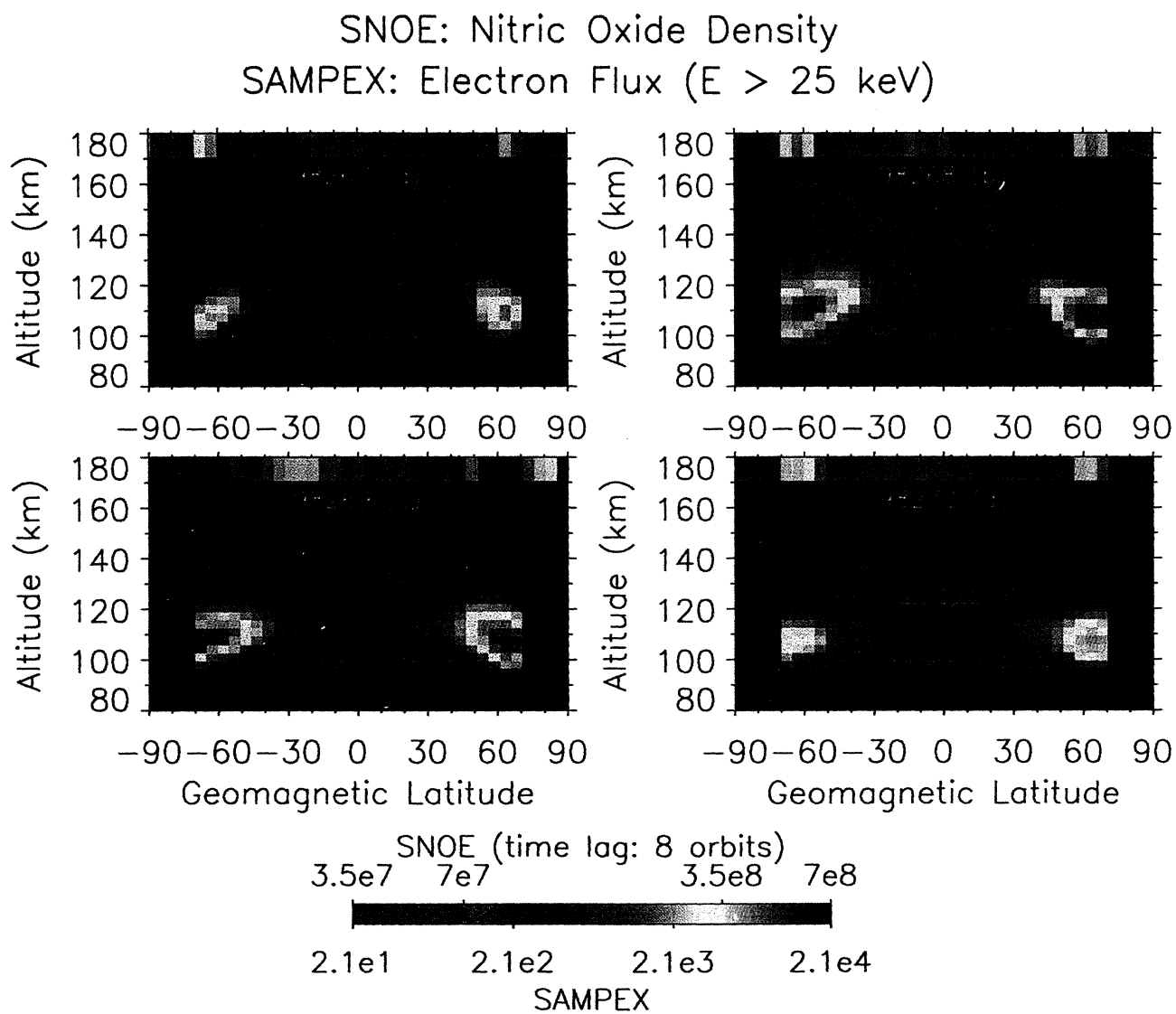**Figure 3.** Similar to Figure 2, but for October 17-24, 1998 (days 290-297).

SAMPEX: Electrons (E > 25.0 keV)

Nitric Oxide Density (106 km)

Day of Year
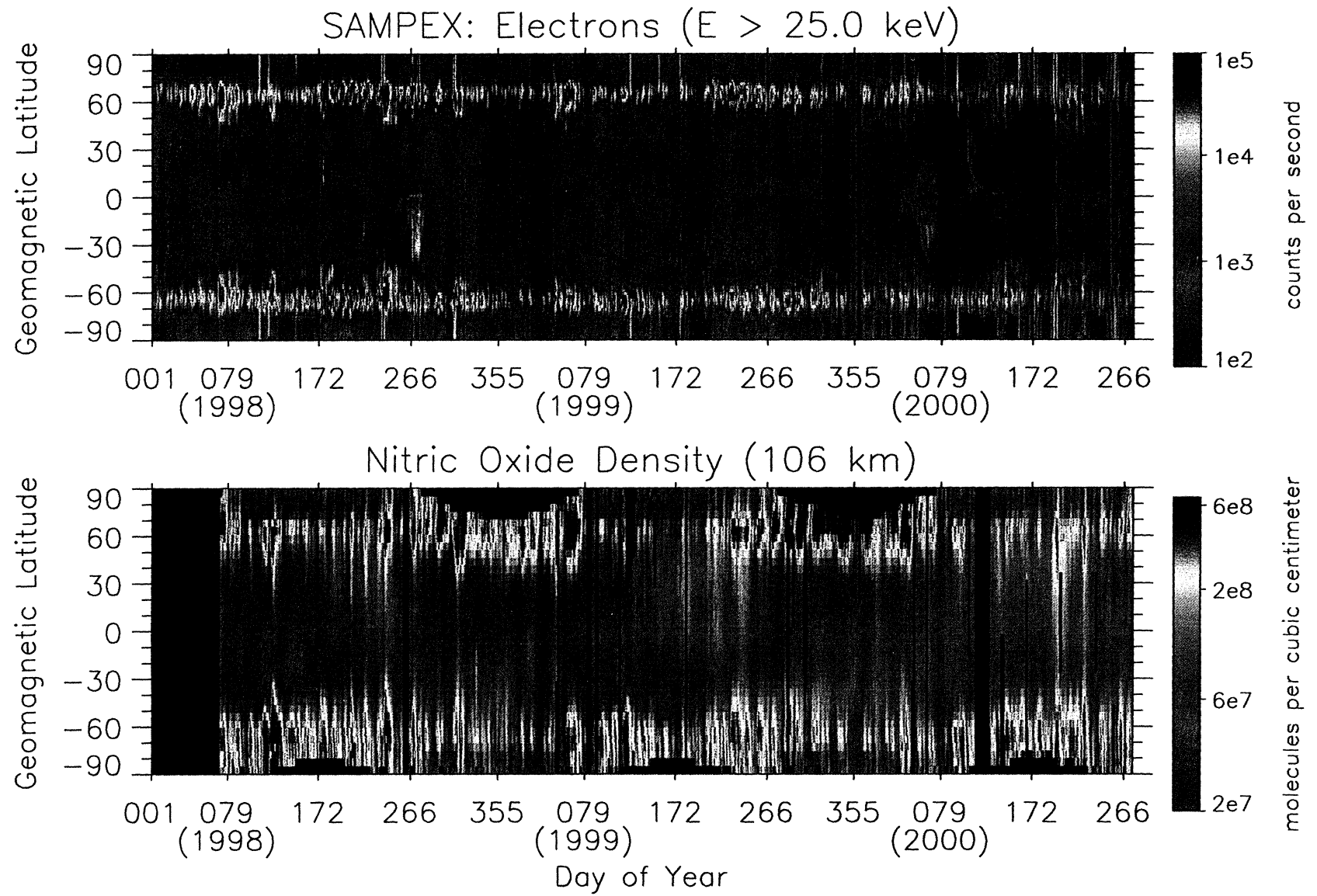
Plate 1. Color-coded counting rates of (top) $E>25$ keV electrons and (bottom) nitric oxide densities at 106 km altitude for 1998-2000. The vertical scale in each panel is geomagnetic latitude and daily-average values are indicated by the color bars to the right. Other details are discussed in the text.

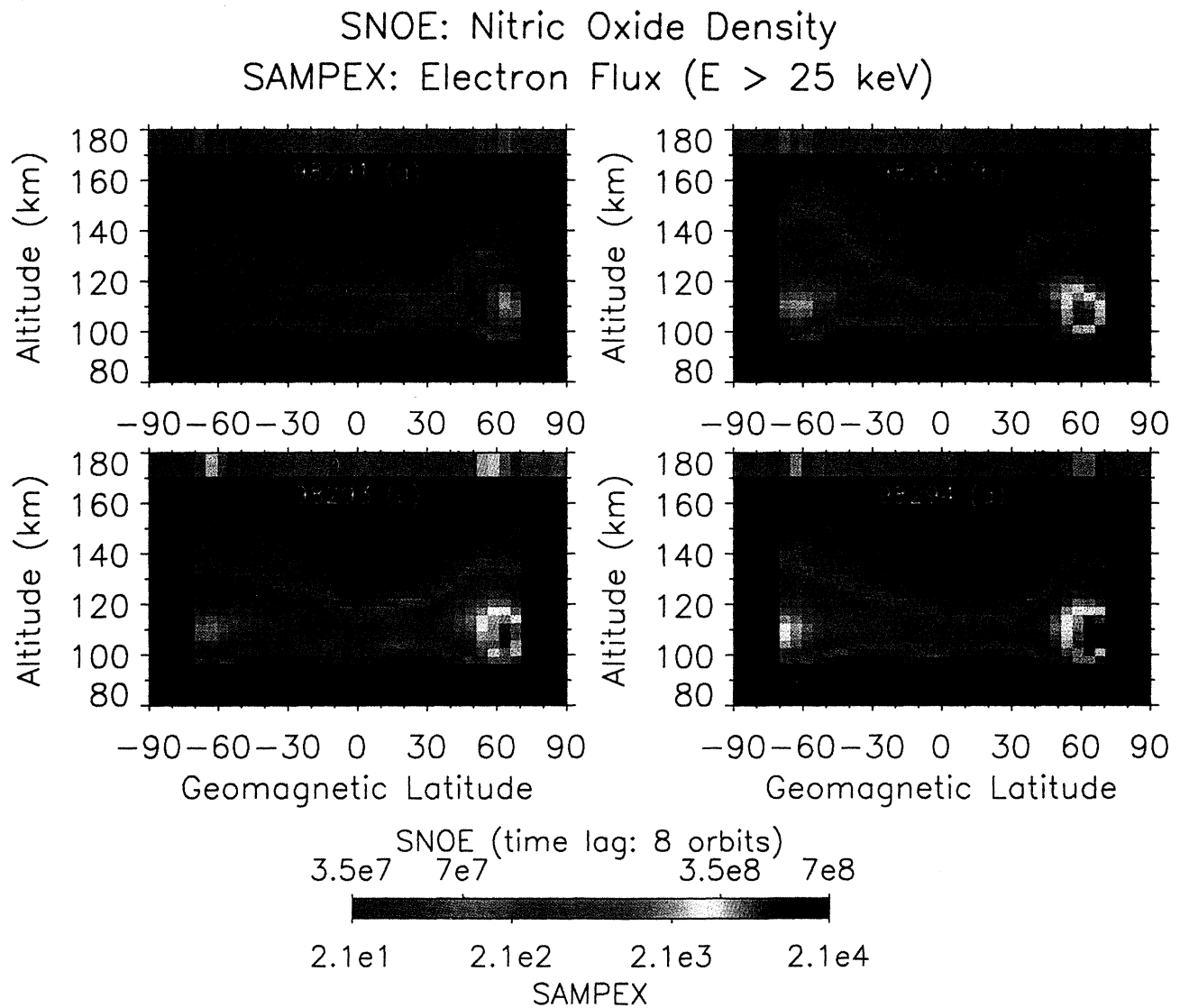## SNOE: Nitric Oxide Density
SAMPEX: Electron Flux (E > 25 keV)
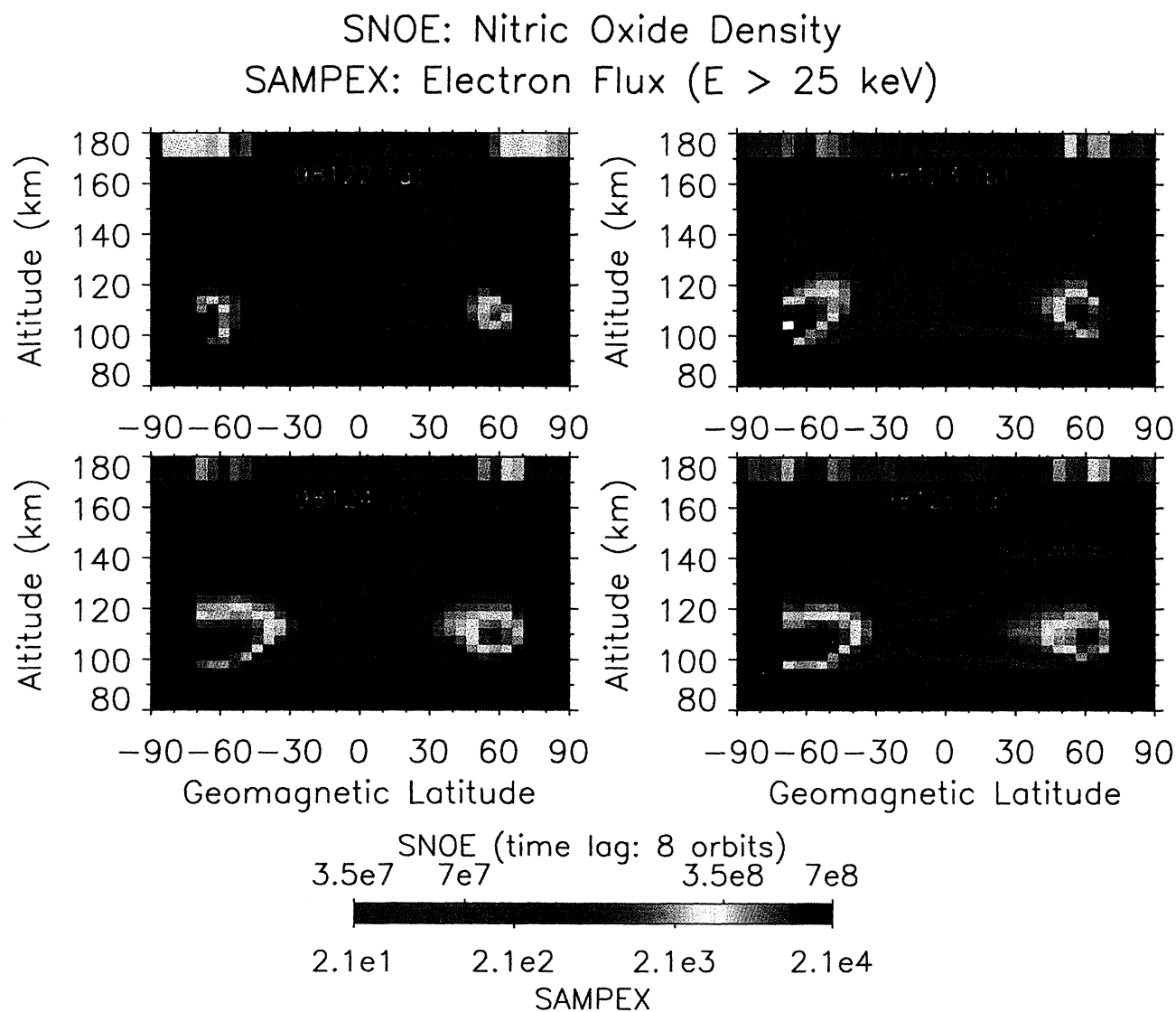
Plate 2. A comparison of Student Nitric Oxide Explorer (SNOE) nitric oxide measurements and the Solar, Anomalous, and Magnetospheric Particle Explorer (SAMPEX) electron (E>25 keV) measurements for days 122 and 125 of 1998 (May 2-5). SNOE data are plotted on a logarithmic scale according to the color scales at the bottom of the figure. The SAMPEX electron counting rates range over several orders of magnitude, as also shown by the color bar. Further details are given in the text. (Adapted from figure presented by *Baker* [2000]).
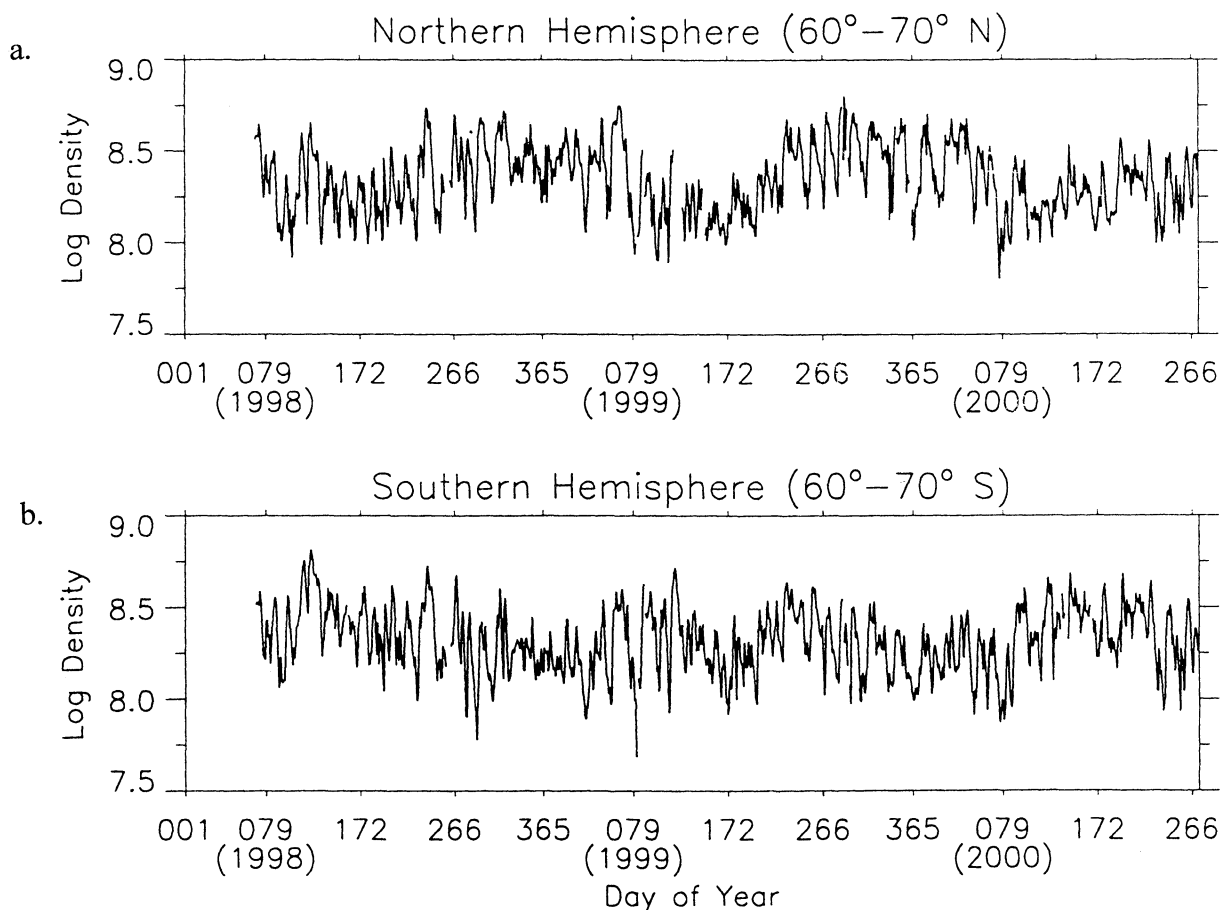
SNOE: Nitric Oxide Density
SAMPEX: Electron Flux (E > 25 keV)

SNOE (time lag: 8 orbits)

3.5e7   7e7   3.5e8   7e8

2.1e1   2.1e2   2.1e3   2.1e4

SAMPEX

Plate 3. Presentation similar to Plate 2, but for September 24 to 27, 1998 (days 267-270).

SNOE: Nitric Oxide Density
SAMPEX: Electron Flux (E > 25 keV)

SNOE (time lag: 8 orbits)

SAMPEX

Plate 4. Similar to Plate 2, but for October 18-21, 1998 (days 291-294).
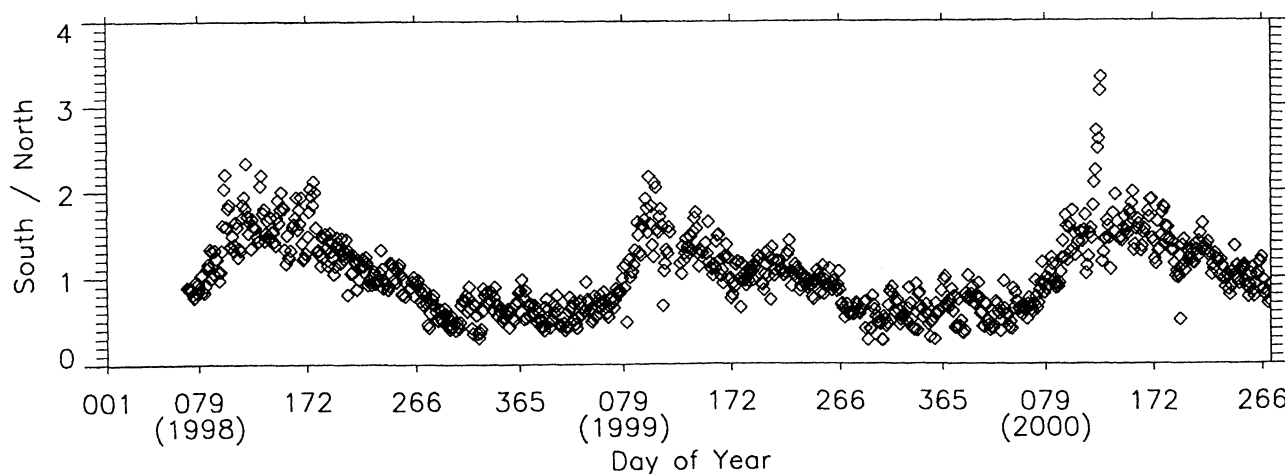
Figure 4. (a) Density of nitric oxide (daily average) measured by SNOE at 106 km altitude in the magnetic latitude band 60°-70° in the Northern Hemisphere for the period day 79 of 1998 to day 79 of 2000. (b) Similar to Figure 4a, but for southern magnetic latitudes (-60° to -70°). Correlation parameters (and fitted lines) are shown in each panel.

SNOE data from this altitude for present studies. We have chosen to use two full years for our studies, namely, day 79 of 1998 to day 79 of 2000.

Figure 4 shows plots of daily-averaged SNOE nitric oxide densities at 106 km altitude. The NO density is plotted in Figure 4a for the northern geomagnetic latitude band 60°-70° versus day of year. Similar values for the southern latitude band (-60° to -

70°) are shown in Figure 4b. Daily average densities range from low values of ~7 x 10^7 cm^{-3} to high values of ~6 x 10^8 cm^{-3}. Note also the tendency for seasonal trends in the data such that NO densities are generally higher in the north in northern winter and are also slightly higher in the south during southern winter. This is plausibly due to greater lifetimes when solar illumination, and related photodissociation, is reduced in the winter hemisphere.

Figure 5. The Southern Hemisphere to Northern Hemisphere ratio of daily averages of nitric oxide shown in Figure 4. A strong seasonal oscillation is seen.

a

b
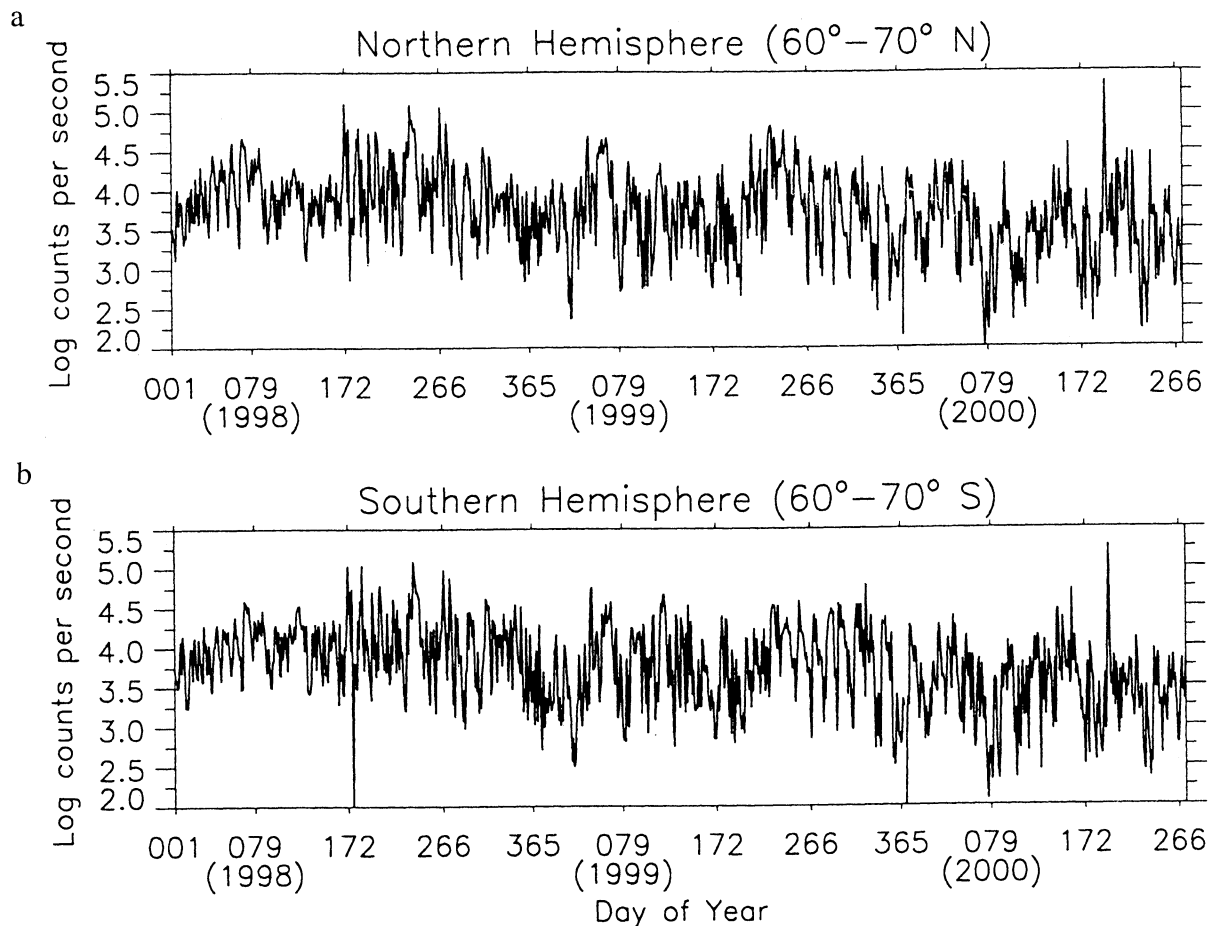
Figure 6. (a) Daily-average counting rates for $E>25$ keV electrons measured by SAMPEX LICA in the magnetic latitude band 60°-70° in the Northern Hemisphere for the period day 79 of 1998 to day 79 of 2000. (b) Similar to Figure 6a, but for southern magnetic latitudes (-60° to -70°).

Figure 5 shows the importance of this effect more explicitly. In this figure, the density of NO in the Southern Hemisphere ($-60° \geq MLAT \geq -70°$) for each day is divided by the corresponding value of NO density in the Northern Hemisphere ($60° \leq MLAT \leq 70°$). The south-to-north ratio shows quite strikingly how the auroral region NO density varies on an annual basis. It is also possible that this asymmetry is due in part to the hemispheric asymmetry that has been observed in auroral particle precipitation [e.g., *Liou et al.*, 1997; *Newell et al.*, 1998; *Petrinec et al.*, 2000] due to sunlight suppression of auroral arcs.

Figure 6 is analogous to Figure 4, but it shows daily average count rates for the LICA $E>25$ keV electrons. Again, the top panel (Figure 6a) shows Northern Hemisphere data (60° to 70° geomagnetic latitude), while the lower panel (Figure 6b) shows Southern Hemisphere data (-60° to -70°). For the electron data, there are not very obvious summer-winter asymmetries as there were for the NO densities. In fact, the Northern and Southern Hemisphere time series look remarkably similar. The counting rates range broadly in Figure 6 from ~5 x 10^2 c/s to ~10^5 c/s. Note, therefore, that electron fluxes range over at least 3 orders of magnitude while the NO densities (Figure 6) range only over about 1 order of magnitude.

It is of interest to examine correlations between the Northern and Southern Hemisphere measurements shown in Figures 4 and 6. Figure 7a presents a scatterplot of NO data with Southern Hemisphere (SH) values indicated by the vertical axis and North-

ern Hemisphere (NH) values indicated by the horizontal axis. As is evident from the data points, the SH and NH SNOE data are fairly broadly distributed. The solid line is a "two-dimensional" power law least squares fit to the data [see *Press et al.*, 1992]. As is seen from the fitted trend line, the best fit line has a somewhat flat slope (SH=1.11 NH $^{0.913}$). This power law (log-log) fit has a correlation coefficient of r=0.503.

Figure 7b shows that the $E>25$ keV electrons are more highly correlated between the two hemispheres. The fitted power law trend line (SH=0.87 NH $^{1.022}$) is relatively close to the unit slope line, and the correlation coefficient is a very high r=0.908. As for the NO data (Figure 7a), the LICA electrons show a slight dominance of SH intensities at low activity and NH intensities at high activity.

Figure 8 shows the relationships that exist between daily-average NO densities and concurrent $E>25$ keV electron count rates. Figure 8a shows the scatter diagram for NH data, and Figure 8b shows SH data. The northern auroral zone data indicate a fairly broad scatter of data points: The fitted power law trend line (NO=8.1 x 10^6 $[F_{elec}]^{0.384}$) has a correlation coefficient of r=0.564. This means that about 32% of the variance ($\propto r^2$) can be accounted for by the NO-electron relationship examined here. On the other hand, the southern auroral zone data are much more highly correlated (Figure 8b). The fitted trend line for the SH data (NO=1.03 x 10^7 $[F_{elec}]^{0.336}$) has a relatively high correlation coefficient of r=0.730. This means that over half the variance of NO

SNOE Nitric Oxide

SAMPEX / LICA Precipitating Electrons
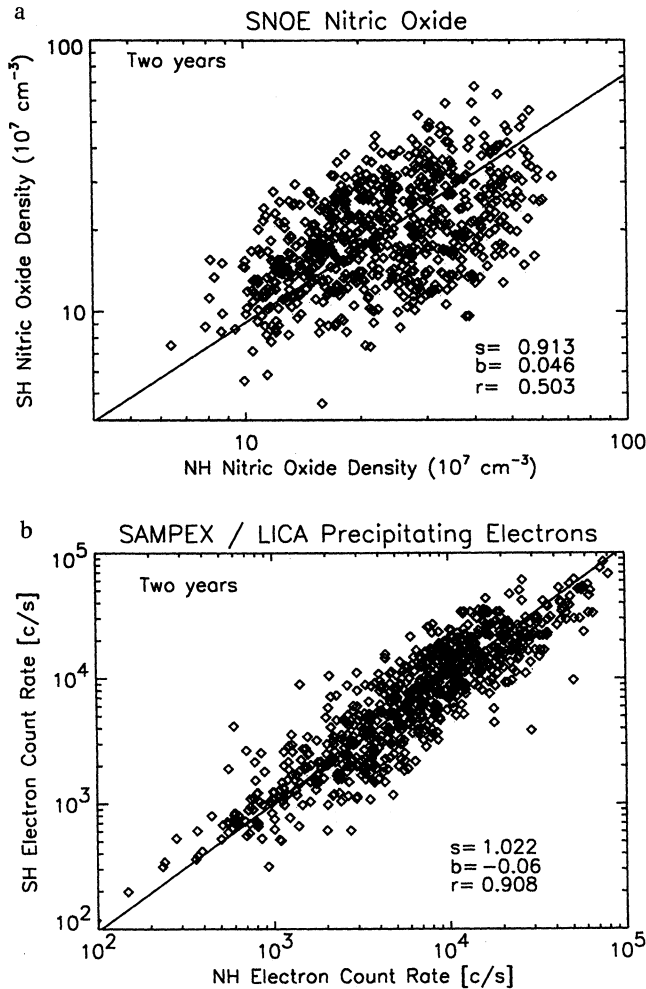
Figure 7. (a) A scatter diagram and two-dimensional least squares fit showing Northern Hemisphere NO densities versus Southern Hemisphere densities (using data from Figure 4). (b) Similar to Figure 7a, but for $E>25$ keV electrons (data from Figure 6).

could be accounted for owing to the auroral electron flux changes.

Because we know that nitric oxide densities at 100-110 km altitudes are produced primarily by ~1-5 keV electrons, we would certainly not expect perfect correlations between SNOE data and the relatively energetic (>25 keV) electrons measured by SAMPEX LICA. In fact, energy spectral variations from event to event in the auroral zone could, in principle, mean that the higher-energy tail of the precipitating electron population could vary in rather different ways than do the bulk of the auroral electrons near E ~1 keV. This led us to consider other spacecraft measurements of lower-energy precipitating electrons for comparison. One convenient, and readily available, data set is the "hemispherical power index" (HPI) obtained by the National Oceanic and Atmospheric Administration (NOAA) TIROS spacecraft [e.g., *Fuller-Rowell and Evans*, 1987]. The HPI estimates the total power coming into the upper atmosphere as a function of time. It is normally dominated by relatively low energy electrons (1-10 keV) and peaks clearly in the auroral zones. The Northern and Southern Hemisphere HPI data are generated separately and were used this way here (data courtesy of D.S. Evans, 2000).

In Figure 9 we compare the daily-averaged SAMPEX $E>25$ keV electron count rates with the NOAA HPI data for the period 1998 (day 79) to 2000 (day 79). The Northern Hemisphere (Figure 9a) and the Southern Hemisphere (Figure 9b) data look remarkably similar, as do the least squares fits. The correlation coefficients for the distributions are $r=0.682$ (NH) and $r=0.696$ (SH). Thus some nearly 50% of the variance of LICA fluxes can be related to the low-energy electrons represented by the HPI values.

As a final statistical comparison, we directly relate the daily-averaged SNOE auroral zone data to the NOAA HPI data. This comparison is shown in Figure 10a (NH) and Figure 10b (SH). Perhaps a little surprisingly, the correlations of SNOE nitric oxide densities and the HPI (r~0.615 and $r=0.643$, north and south, respectively) are not very much better than the correlations obtained between SNOE and SAMPEX LICA (see Figure 8). In fact, for the Southern Hemisphere case, the SNOE-SAMPEX correlation is actually better than is the SNOE-HPI correlation.

6. Discussion and Conclusions

In this paper we have intercompared nitric oxide data and energetic particle data using daily-averaged measurements. Initial comparisons were made between NO densities measured by

SNOE / SAMPEX Comparison

SNOE / SAMPEX Comparison
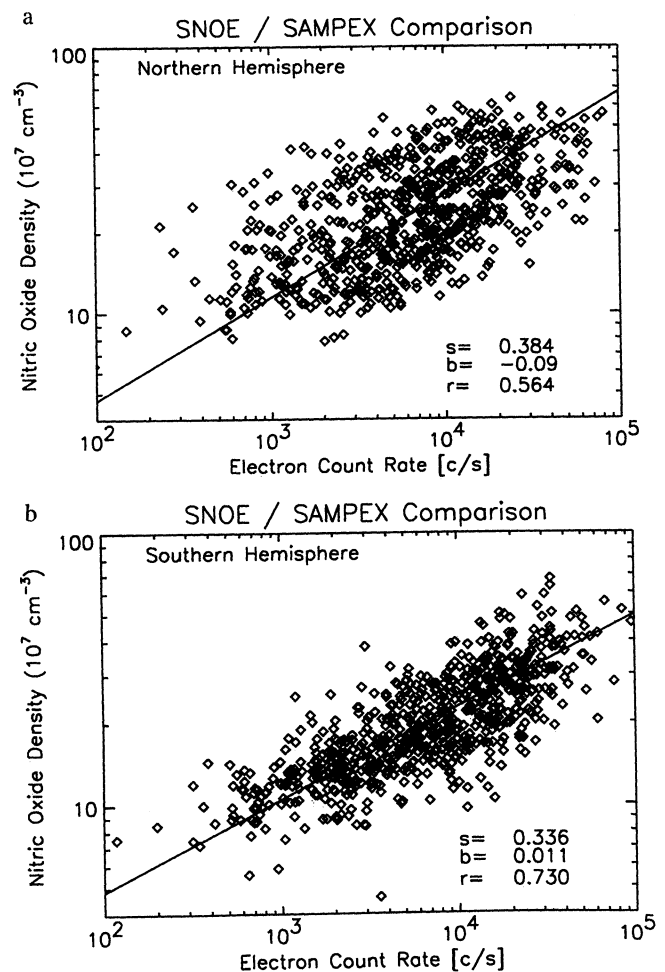
Figure 8. (a) Scatter diagram between Northern Hemisphere NO densities and concurrent $E>25$ keV electron count rates using daily averages from Figure 4a and from Figure 6a, respectively. (b) Similar to Figure 8a, but using Southern Hemisphere daily averages (Figures 4b and 6b).

a

SAMPEX / NOAA Comparison

b

SAMPEX / NOAA Comparison
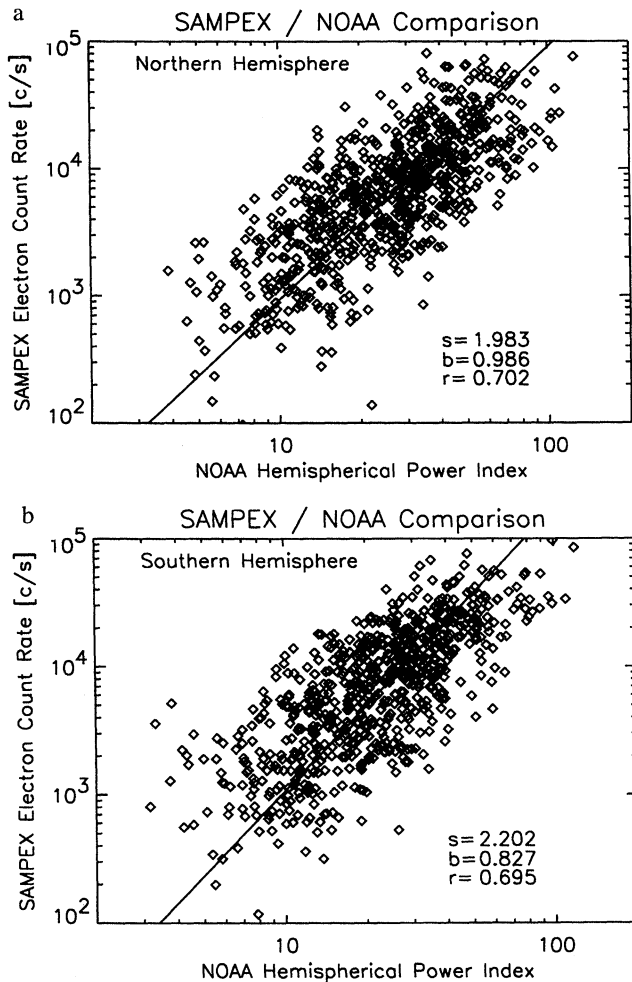
Figure 9. (a) Scatter diagram and least squares fit between Northern Hemisphere $E>25$ keV count rate averages and the daily average National Oceanic and Atmospheric Administration (NOAA) "hemisphere power index" discussed in the text. (b) Similar to Figure 9a for the Southern Hemisphere.

SNOE sensors and particle fluxes measured using SAMPEX sensors: These two spacecraft operate at about the same altitude, but in general are in different orbital planes. Nonetheless, the similarly complete data in magnetic latitude (and continuous measurements in time at similar altitudes) made daily comparisons interesting and valuable. We have found that $E>25$ keV electron counting rates are relatively north-south symmetric between the two auroral zones, but the nitric oxide densities show much more north-south asymmetry. As speculated in the data presentation above (see Plate 1) and as shown more clearly in Figure 5, this north-south asymmetry probably is due, at least in part, to the amount of solar UV reaching the high-latitude regions and the resulting photodissociation of NO that does (or does not) occur during different seasons of the year.

It seems evident that a model that included the seasonal NO lifetime discussed here could potentially improve the correlations between particle energy inputs and resultant NO densities. A seasonal and latitudinal "correction" for the daily values of NO would lead to more linear relationships with precipitating particle flux measurements. Using the kind of seasonal dependence of NO densities revealed by Figure 5, we have made a simple (sinusoidal in time) model to account for north-south asymmetries.

The seasonal correction gives NO densities that should better correlate with particle measurements. Figure 11 shows that this is, indeed, the case (at least for SAMPEX data). Figure 11a shows Northern Hemisphere correlation between SNOE and LICA data: The correlation coefficient is found to be $r=0.690$. The uncorrected correlation, recall (Figure 8a), was $r=0.564$. Figure 11b shows the SNOE versus NOAA HPI data for the Northern Hemisphere: The correlation coefficient is $r=0.629$. Previously, prior to the seasonal correction, the value was $r=0.615$, so a slight positive difference results. The Southern Hemisphere correlations between corrected NO densities and LICA ($r=0.718$) and HPI ($r=0.719$) are even a bit higher than for the Northern Hemisphere (scatter diagrams not shown here). Having made some correction for seasonal NO dependences, we look forward in future work to studying seasonal particle precipitation dependences as discussed, for example, by *Newell et al.*, [1998].

From energy deposition versus altitude considerations, we are well aware that $E>25$ keV electrons deposit their energy in the altitude range ~90 km and below [see *Codrescu et al.*, 1997]. On the other hand, the data presented in this paper show that nitric oxide densities are highest at altitudes above 100 km. Thus the comparison of NO densities at 106 km altitudes with electron intensities measured by SAMPEX LICA is a bit of a mismatch. It was for this reason that we elected to also use NOAA HPI data

a

SNOE / NOAA Comparison

b

SNOE / NOAA Comparison
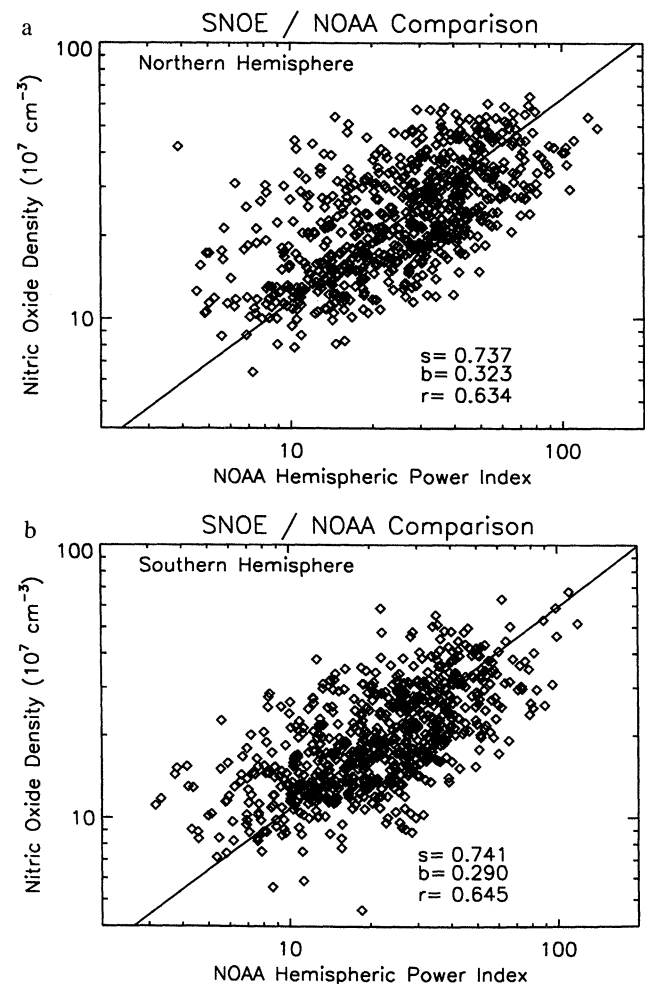
Figure 10. (a) Scatter diagram and least squares fit for Northern Hemisphere nitric oxide densities and the daily average NOAA hemispherical power index. (b) Similar to Figure 10a for the southern hemisphere.

a

SNOE / SAMPEX Comparison

b

SNOE / NOAA Comparison
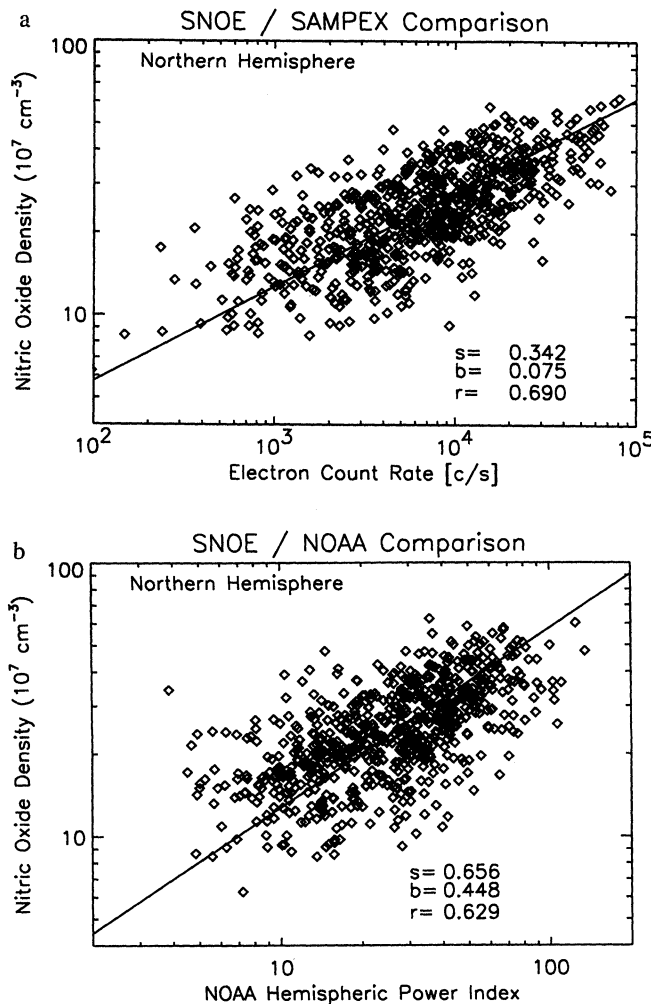
Figure 11. (a) Scatter diagram and least squares fit for Northern Hemisphere nitric oxide densities corrected for seasonal variations versus SAMPEX-measured electrons with $E>25$ keV. (b) Similar to Figure 11a, but now plotting corrected NO densities versus the NOAA hemispherical power index.

for comparison to SNOE data. Yet, as our analysis has shown, we do not find any better correlation using HPI data than we do using LICA data: All our cross correlations are in the ~0.6 to ~0.7 range. This means that about 35% to 50% of the variance can be accounted for by the statistical relationships explored here. Many other factors, including measurement time differences, local time dependences, spectral effects, and other factors, probably account for the less than perfect correlation observed.

We have commented in the data presentation above that the NO densities vary over the course of a year by about a factor of 10. It is clear that the NOAA HPI data vary a bit more than this (see Figures 9 and 10), perhaps showing a dynamic range of a factor of ~25. On the other hand, the $E>25$ keV electron counting rates vary by a factor of perhaps 400 or so. This fact emphasizes further that the spectrum of electrons precipitating into the upper atmosphere probably has a low-energy peak in differential flux (or number flux) near ~1 keV that is more steady in value with a high-energy spectral "tail" that varies much more widely. The bulk of the auroral electrons (near 1 keV) are correlated with the $E>25$ keV electrons, but the correlation is probably only in the 0.6-0.7 range.

Several recent papers have reported on nitric oxide measurements from the Halogen Occultation Experiment (HALOE) on board the Upper Atmosphere Research Satellite (UARS) [Crowley et al., 1998, 1999; Ridley et al., 1999]. HALOE measures nitric oxide at sunrise and sunset at latitudes and longitudes that vary systematically over a 34-day period. HALOE is able to cover magnetic latitudes from 73°S to 68°N over this interval of time. In the course of a 34-day period, the HALOE experiment covers many different magnetic local times. UARS also measures on the same platform the particle fluxes and spectra [e.g., *Frahm et al.*, 1997]. As we have described, SNOE samples a broader range of magnetic latitudes (nearly pole to pole) at all geographic longitudes, but only at 1030 LT. Thus SNOE and UARS HALOE are in some senses complementary in their measurements.

Crowley et al. [1998] described a geomagnetic storm interval (12 days) and showed a variation of NO as a function of geographic longitude. *Crowley et al.* [1999] reported that hemispheric asymmetries of NO that appear when plotted in geographic coordinates disappear when plotted in geomagnetic coordinates. In our Plates 2, 3, and 4 we have used geomagnetic coordinates, but N-S asymmetries persist (at times both in NO and in particle fluxes). *Ridley et al.* [1999] presented a 5 year statistical analysis of NO data. They found a clear local time asymmetry. We are unable to perform such local time analysis with SNOE, but we can make other direct comparisons with HALOE. We look forward to such comparisons.

In summary, we wish to emphasize that understanding the coupling of magnetospheric particle populations into the upper atmosphere of the Earth is crucially important to arrive at a true comprehension of the Sun-Earth connection. Until we understand fully the role of magnetosphere-atmosphere linkages and the chemical changes induced thereby, we cannot hope to appreciate fully the role of natural variability in global atmospheric changes. We feel that long-term, continuous data from spacecraft such as SNOE, SAMPEX, and TIROS can play a key role in arriving at such an understanding of Sun-Earth connections.

References

Baker, D.N., Effects of the Sun on the Earth's environment, *J. Atmos. Sol. Terr. Phys., 62,* 1669, 2000.

Baker, D.N., J.B. Blake, D.J. Gorney, P.R. Higbie, R.W. Klebesadel, and J.H. King, Highly relativistic magnetospheric electrons: A role in coupling to the middle atmosphere, *Geophys. Res. Lett., 14,* 1027, 1987.

Baker, D.N., G.M. Mason, O. Figueroa, G. Colon, J.G. Watzin, and R.M. Aleman, An overview of the Solar, Anomalous, and Magnetospheric Particle Explorer (SAMPEX) mission, *IEEE Trans. Geosci. Remote Sens., 31,* 531, 1993.

Baker, D.N., J.H. Allen, S.G. Kanekal, and G.D. Reeves, Disturbed space environment may have been related to pager satellite failure, *Eos Trans. AGU, 79,* 477, 1998.

Baker, D.N., N.E. Turner, and T.I. Pulkkinen, Energy transport and dissipation in the magnetosphere during geomagnetic storms, *J. Atmos. Sol. Terr. Phys., 63,* 421, 2001.

Barth, C.A., Nitric oxide in the lower thermosphere, *Planet. Space Sci., 40,* 315, 1992.

Barth, C.A., S.M. Bailey, and S.C. Solomon, Solar-terrestrial coupling: Solar soft X-rays and thermospheric nitric oxide, *Geophys. Res. Lett., 26,* 1251, 1999.

Barth, C.A., D.N. Baker, K.D. Mankoff, and S.M. Bailey, The northern auroral region as observed in nitric oxide, *Geophys. Res. Lett., 28,* 1463, 2001.

Callis, L.B., D.N. Baker, J.B. Blake, J.D. Lambeth, R.E. Boughner, M. Natarajan, R.W. Klebesadel, and D.J. Gorney, Precipitating relativistic electrons: Their long-term effect on stratospheric odd nitrogen levels, *J. Geophys. Res., 96,* 2939, 1991.

Callis, L.B., D.N. Baker, M. Natarajan, J.B. Blake, R.A. Mewaldt, R.S. Selesnick, and J.R. Cummings, A 2-D model simulation of downward transport of NO_y into the stratosphere: Effects on the 1994 austral spring O_z and NO_y, *Geophys. Res. Lett., 23,* 1905, 1996.

Callis, L.B., M. Natarajan, J.D. Lambeth, and D.N. Baker, Solar atmospheric coupling by electrons (SOLACE), 2, Calculated stratospheric effects of precipitating electrons, 1979-1988, *J. Geophys. Res., 103,* 28,421, 1998.

Codrescu, M.V., T.J. Fuller-Rowell, R.G. Roble, and D.S. Evans, Medium energy particle precipitation influences on the mesosphere and lower thermosphere, *J. Geophys. Res., 102,* 19,977, 1997.

Crowley, G., A. Ridley, D. Winningham, R. Frahm, J. Sharber, J. Russell III, and R.G. Roble, Nitric oxide variations in the mesosphere and lower thermosphere during the November 1993 storm period, *J. Geophys. Res., 103,* 26,395, 1998.

Crowley, G., A. Ridley, D. Winningham, R. Frahm, J. Sharber, J. Russell III, and R.G. Roble. On the hemispheric symmetry in thermospheric nitric oxide, *Geophys. Res. Lett., 26,* 1545, 1999.

Crutzen, P.J., I.S.A. Isaksesn, and G.C. Reid, Solar proton events, stratospheric sources of nitric oxide, *Science, 189,* 457, 1975.

Frahm, R.A., et al., The diffuse aurora: A significant source of ionization the middle atmosphere, *J. Geophys. Res., 102,* 28,203, 1997.

Fuller-Rowell, T.J., and D.S. Evans, Height-integrated Pederson and Hall conductivity patterns inferred from the TIROS-NOAA satellite data, *J. Geophys. Res., 92,* 7606, 1987.

Lean, J., et al., *Solar Influences on Global Change,* National Research Council report, Natl. Acad. of Sci. Press, Washington, D.C., 1994.

Liou, K., P.T. Newell, C.-I. Meng, M. Brittracher, and G. Parks, Synoptic auroral distribution: A survey using Polar ultraviolet imagery, *J. Geophys. Res., 102,* 27,197, 1997.

Lu, G., et al., Global energy deposition during the January 1997 magnetic cloud event, *J. Geophys. Res., 103,* 11,685, 1998.

Mason, G.M., et al., LEICA: A low-energy ion composition analyzer for the study of solar and magnetospheric heavy ions, *IEEE Trans. Geosci. Remote Sens., 31,* 549, 1993.

McAdams, K.L., and G.D. Reeves, Non-adiabatic response of relativistic radiation belt electrons to GEM magnetic storms, *Geophys. Res. Lett., 28,* 1897, 2001.

Newell, P.T., C.I. Meng, and S. Wing, Relation to solar activity of intense aurorae in sunlight and darkness, *Nature, 393,* 342, 1998.

Petrinec, S.M., W.L. Imhof, D.L. Chenette, J. Mobilia, and T.J. Rosenberg, Dayside/nightside auroral X-ray emission differences: Implication for ionospheric conductance, *Geophys. Res. Lett., 27,* 3277, 2000.

Press, W.H., S.A. Teukolsky, W.T. Vetterling, and B.P. Flannery, *Numerical Recipes in FORTRAN,* Cambridge Univ. Press, New York, 1992.

Randall, C.E., D.W. Rusch, R.M. Bevilacqua, K.W. Hoppel, and J.D. Lumpe, POAM II stratospheric NO_2, 1993-1996, *J. Geophys. Res., 103,* 28,361, 1998.

Ridley, A.J., G. Crowley, R. Frahm, D. Winningham, J. Sharber, J. Russell III, and R.G. Roble, Variations of the nitric oxide mass mixing ratio in the thermosphere as a function of Kp, *Geophys. Res. Lett., 26,* 1541, 1999.

Roble, R.G., The polar lower thermosphere, *Planet. Space Sci., 40,* 271, 1992.

Thorne, R.M., Energetic radiation belt precipitation: A natural depletion mechanism for stratospheric ozone, *Science, 21,* 287, 1977.

S.M. Bailey, Center for Atmospheric Sciences, Hampton University, 23 Tyler Street, Hampton, VA 23668, USA.

D.N. Baker, C.A. Barth, S.G. Kanekal, and K.E. Mankoff, Laboratory for Atmospheric and Space Physics, University of Colorado, 1234 Innovation Drive, 590 UCB, Boulder, CO 80309-0590, USA (daniel.baker@lasp.colorado.edu).

G.M. Mason, Department of Physics, University of Maryland, College Park, MD 20742, USA.

J.E. Mazur, Aerospace Corporation, 2350 E. El Segundo Blvd., El Segundo, CA, 90245-4691, USA.